Analyst

Accepted Manuscript

ROYAL SOCIETY OF CHEMISTRY

www.rsc.org/analyst

Ion Mobility-Mass Spectrometry of Charge-Reduced Protein Complexes Reveals General Trends in the Collisional Ejection of Compact Subunits

Russell E. Bornschein, Brandon T. Ruotolo*

Department of Chemistry, University of Michigan, 930 N. University Ave., Ann Arbor, MI 48109

*To Whom Correspondence should be addressed: bruotolo@umich.edu, [V] 734-615-0198, [F] 734-615-3718

Abstract

Multiprotein complexes have been shown to play critical roles across a wide range of cellular functions, but most probes of protein quaternary structure are limited in their ability analyze complex mixtures and polydisperse structures using small amounts of total protein. Ion mobility-mass spectrometry offers a solution to many of these challenges, but relies upon gas-phase measurements of intact multiprotein complexes, subcomplexes, and subunits that correlate well with solution structures. The greatest bottleneck in such workflows is the generation of representative subcomplexes and subunits. Collisional activation of complexes can act to produce product ions reflective of protein complex composition, but such product ions are typically challenging to interpret in terms of their relationship to solution structure due to their typically string-like conformations following activation and subsequent dissociation. Here, we used ion-ion chemistry to perform a broad survey of the gas-phase dissociation of charge-reduced protein complex ions, revealing general trends associated with the collisional ejection of compact, rather than unfolded, protein subunits. Furthermore, we also discover peptide and co-factor dissociation channels that dominate the product ions populations generated for such charge reduced complexes. We assess both sets of observations and discuss general principles that can be extended to the analysis of protein complex ions having unknown structures.

Introduction

Macromolecular protein complexes play a critical role in carrying out most of the key functions within the cell, from synthesis to cell death.[1] The quaternary structures of these multiprotein machines, therefore, are key targets for structural biology, in that such information can often lead to breakthroughs in human health and disease treatments.[2,3] High-resolution methods aimed at the direct collection of protein structure information, such as X-ray diffraction (XRD) and nuclear magnetic resonance (NMR) spectroscopy, are often limited by stringent sample requirements in terms of purity, amount, protein flexibility, and assembly polydispersity.[4] Multiple mass spectrometry (MS) techniques are poised to overcome many of these challenges, and contribute toward a high-throughput lower-resolution protein complex structure pipeline able to access the proteome comprehensively.[5] Approaches such as ion mobility (IM),[6,7] chemical cross-linking (CXL),[8,9] and hydrogen/deuterium exchange (HDX),[10-12] when coupled to MS, have the ability to probe protein secondary, tertiary, and quaternary structure in addition to primary structure, thus enabling the generation of models of protein architecture in cases where classical structural biology tools provide little information.

Ion mobility-mass spectrometry (IM-MS) is unique amongst the technologies listed above, in that protein structures are probed entirely in the gas-phase. Experimental evidence has demonstrated that native-like gas-phase conformations can be retained during nanoelectrospray ionization (nESI) when neutral pH, volatile aqueous buffers are used as solvents.[6,13-15] From IM-MS data, both stoichiometry and size (*via* measured collision cross-section; CCS) information can be determined and used to build low-resolution coarse-grain model structures of multiprotein assemblies.[16-18] However, in order to build these coarse-grain topology models, the sizes of subunits and subcomplexes must be measured in the gas-phase, and these assemblies must

possess native-like conformations that are strongly-correlated with solution structures. Disruption of multiprotein complexes can be initiated in solution, through the alteration of ionic strength, solvents composition, and pH.[19,20] While such approaches are currently the most reliable and broadly applied method for generating structurally-informative subcomplexes for protein complex model construction, broad application of solution-phase disruption IM-MS is currently hampered by an incomplete mechanistic understanding of subcomplex formation and protein-dependant responses to specific disruption agents.[15,18,19,21-23] Alternatively, gas-phase dissociation methods, such as collision induced dissociation (CID)[24] and surface induced dissociation (SID),[25] are a promising class of techniques that potentially enable the targeted, universal production of subcomplex information for protein complex modeling efforts. However, for the vast majority of protein complex ions, CID usually results in the generation of highly-unfolded monomeric product ions following an asymmetric charge partitioning mechanism, where the monomer carries a disproportionate amount of the parent ion charge relative to mass.[26-28] IM measurements for such ions are not typically useful for building protein structure models due to collision induced unfolding (CIU), and thus controlling the conformation of the product ions produced from intact protein assemblies is a challenge for gas-phase structural biology.[28]

Recently, CID of a charge-reduced protein complex was observed to produce compact, native-like monomer product ions.[29] Under such conditions, CID products can be used for building topology models.[29] Previous studies of this altered CID pathways have largely been conducted using solution-phase charge state manipulation techniques, which ultimately limits the number of total assemblies and compact protein charge states screened.[29,30] To fully utilize such CID CCS information for high-throughput structural biology, the level of charge reduction

necessary to alter the CID pathway toward the ejection of compact protein building blocks must be comprehensively characterized in order to generate predictive trends. Previously, we described a continuous gas-phase ion-neutral charge reduction source,[30] and observed compact charge reduced protein complexes formed by a process that was both more effective but less efficient than those generated by solution-phase and ion-ion approaches. Often, the ability to generate multiprotein models from IM-MS data hinges on the ability to produce size estimates of the interacting proteins, some of which cannot be access through protein complex disruption in solution.[16,17,19] As such, any approach capable of enabling the acquisition of such subunit size data would be highly enabling for MS-based structural biology.

Here, we adapt a recently-described corona discharge probe (CDP)[31] to broadly and efficiently study the amount of charge reduction necessary to alter the CID pathways of protein-protein complexes. We find a positive correlation between the threshold charge required to generate compact product ions from CID and the intact molecular mass of the precursor ion selected, for a broad array of protein complexes. In addition, we discover that for the β-galactosidase and catalase tetramers, the energetic barriers associated with peptide bond dissociation becomes either lower or iso-energetic to those associated with compact protein ejection for charge-reduced protein complexes. We analyze and discuss these results in light of their general utility for protein complex structure analysis.

Experimental

Sample Preparation

Ammonium acetate and triethylammonium acetate (TEAA) were purchased from Sigma Aldrich (St. Louis, MO). Aldolase (rabbit muscle, tetramer 157 kDa), avidin (chicken egg white,

tetramer 64 kDa), β-galactosidase (β-Gal; E. coli, tetramer 466 kDa), β-lactoglobulin (β-Lac; bovine, monomer 18.6 kDa and dimer 37 kDa), catalase (bovine, tetramer 233 kDa), concanavalin A (ConA; jack bean, tetramer 103 kDa), cytochrome c (CytC; equine, monomer 12.3 kDa), hemoglobin (Hgb; bovine, dimer 32.4 kDa and tetramer 64.8 kDa), serum amyloid P (SAP; human, pentamer 125 kDa), and triosephosphate isomerase (TPI; rabbit muscle, dimer 53.3 kDa) were selected for this study due to their broad range of masses, various complex stoichiometries, and well documented x-ray crystal structures. All proteins were purchased (Sigma Aldrich) as lyophilized powder. Stock samples were prepared into ammonium acetate at various concentrations. CytC was prepared to a final concentration of 10 μM in 49.5% water:49.5% methanol:1% trifluoroacetic acid (TFA). All other proteins were prepared to a final concentration of 10 μM (with the exception of TPI which had a final concentration of 20 μM) in 200mM ammonium acetate following buffer exchange using Bio-Rad spin columns (Hercules, CA, USA). Alcohol dehydrogenase (ADH; yeast, 153 kDa), glutamic dehydrogenase (GDH; bovine, 336 kDa) and pyruvate kinase (PK; rabbit, 237 kDa) were also prepared for collision cross-section (CCS) calibration.

Instrumentation and Data Analysis

Ion mobility-mass spectrometry (IM-MS) experiments were performed on a commercially available Waters Synapt G2 HDMS (Manchester, UK) platform with a modified nESI source for performing gas-phase ion-ion charge reduction (see below). IM-MS data was processed using MassLynx and Driftscope software (Waters) to measure unknown CCS values following an established protocol[32] using calibrants of known CCS values.[33]

Definitions of charge reduction efficiency and effectiveness used here are identical to those described previously.[30] Briefly, charge reduction efficiency refers to the amount of charge

reduction agent required to reduce protein ion charge states by a fixed amount, whereas charge reduction effectiveness refers to the ultimate amount of charge reduction observed under any set of conditions tested. To determine CID thresholds, the relative parent ion and product ion intensities were evaluated at each collision energy. The CID threshold is defined by the energy at which the product ion intensity reaches 50% (or 50% of the steady state intensity). To determine CIU thresholds, the drift time of the most abundant peak is identified at each collision energy. The CIU threshold is defined by the energy at which the drift time of the most intense peak is 2.5% longer than the shortest observed drift time across all energies, as not all ions studied here generated larger shifts in CCS. In addition, this approach allows for more streamlined data analysis that is consistent with more robust, first-order derivative approaches. CID and CIU thresholds are screened simultaneously across analyte charge states to identify the charge state at which the CID and CIU thresholds converge to the same energy, or invert when the CID threshold occurs at a lower energy than the CIU threshold.

Corona Discharge Charge Reduction

A CDP for performing gas-phase ion-ion charge reduction was constructed based on a previously described design.[31] Briefly, a steel tube with a plastic cuvette attached to one end was mounted onto the nESI source housing in-line with the sampling cone, where the cuvette end is nearest the cone. Mounted to the open end of the cuvette is a grounded 0.5 mm thick stainless steel plate with a 1.5 mm aperture. Contained in the steel tube is a PTFE tube (0.030 inch i.d., 1/16 inch o.d.; Fisher Scientific) containing a 0.368 mm diameter platinum wire (Fisher) with one end ground to a fine point. The fine-point end of the platinum wire is positioned in a point-to-plane geometry with the stainless steel plate at a distance of 1.5-2.5 mm (see *Suplimental Figure S1* for images of complete CDP assembly). The other end of the platinum wire is

connected to a negative high-voltage power supply (Stanford Research Systems, Sunnyvale, CA) through a 25 MΩ resistor (Newark Ohmite, Chicago, IL). Nitrogen gas is split into the PTFE tubing through a PEEK tee (Fisher). The external surface of the stainless steel plate was positioned approximately 1.5 cm from the sampling cone. Gas pressure and applied voltages were varied between 60 to 90 psi and -6500 to -8500 V, respectively.

Results and Discussion

CDP-nESI Source Optimization

Samples containing denatured CytC were used to optimize CDP conditions for maximum charge reduction while maintaining signal intensity. Screened variables include CDP gas pressure, applied voltage, sampling cone voltage and source backing pressure. Representative, optimized MS data from these screens are shown in Figure 1. Higher CDP voltages (Figure 1a) and pressures (Figure 1b) resulted in greater shifts in charge state distributions (CSDs) to lower charge states but at a significant cost to signal intensity, while lower pressures and voltages produce less significant shifts in CSDs with little cost to signal intensity. This tuning effect likely stems from balancing the transmission efficiency of the CDP ion source with the ability to sufficiently collisionally-activate ions post-CDP to dissociate charged species from the analyte protein. To balance the shift in CSDs with ion transmission, the gas pressure and applied voltages were optimized to 70 psi and -7250 V, respectively. Lower charge states are characterized by broader, low intensity MS peaks with higher mass shifts, likely to due to anion attachment from the CDP. To promote collisional cleaning, mild in-source activation was applied by raising the sampling cone voltage and lowering the backing pressure. Higher sampling cone voltages had little effect on signal intensity, and was therefore optimized to the maximum value

of 200 V to aid in adduct reduction. Backing pressure (Figure 1c) proved to have a significant effect on both the CSD and the level of adduction. For studying intact protein complexes, lower backing pressures had a significant effect on signal intensity, and therefore pressure was optimized at approximately 7 mbar for such larger ions. Drift times of the low charge states of interest were monitored throughout the collisional cleaning process and no significant ion CCS changes were observed under these conditions, indicating compact gas-phase structures are retained.

Under the conditions described above, the extent of charge reduction for intact protein complexes was assessed. Figure 2 presents optimized data from these screens (for additional proteins see *Supplemental Figures S2 to S7*). Under control nESI conditions, the most intense peaks for the monomeric and dimeric forms of β-Lac (Figure 2a, bottom) correspond to the 7^+ and 12^+ charge states, respectively. Using the optimized charge reduction conditions described above, the most intense peaks for β-Lac shift to the 5^+ and 9^+ charge states for monomer (middle) and dimer (top), respectively, with the lowest observed charge states being 4^+ for both monomer and dimer (note monomer and dimer CDP spectra have been deconvoluted through post-mobility data processing). In the case of the TPI dimer (Figure 2b), the lowest charge state shifts from 13^+ to 8^+ upon activation of the CDP, while the most intense peak remains constant at the 15^+ charge state. Similarly, for the SAP pentamer (Figure 2c), while the most intense peak remains the 24^+ under both conditions, the lowest observed charge state shifts from 22^+ to 11^+ when the CDP is activated. Interestingly, we observe a minor increase in the most intense charge state for β-Gal, which shifts from 47^+ to 49^+ upon CDP activation, however, as expected the lowest observed charge state decreases from 44^+ to 36^+. While these data demonstrate some differences in the CSD shifts observed, all proteins show significant evidence of charge reduction. Structural

effects from in-source activation used to aid in charge stripping were monitored through a comparison of CCS measurements acquired under control native MS conditions and demonstrated good agreement between overlapping low charge states (see *Supplemental Table S1*). While higher charge states did display evidence of unfolding in our experiments, the low charge state ions of interest maintained compact conformations under a broad set of instrumental conditions. Stated specifically, our optimized conditions appear effective for different complexes, across a broad range of masses (18.6 to 466 kDa) and assembly stoichiometries (monomers to pentamers).

While TEAA addition in solution was, overall a more effective method of charge reduction when compared with the CDP source used in these studies, we observed two examples where CDP was the more effective approach. For example, we typically observe the 11^+ as the lowest observable charge state of the avidin tetramer using TEAA in solution,[34] while 8^+ ions were generated with moderate intensity using the CDP source (see *Supplemental Figure S2*). Similarly, using TEAA to charge reduce aldolase[34] generated ions with charges as low as 17^+, but using the CDP generated extending to 14^+ ions (see *Supplemental Figure S3*). Despite minor limitation, therefore, we find the CDP approach to be a generally flexible and effective approach toward protein complex charge reduction, which provides a universal approach capable of reducing the charge state of a broad range of assemblies, independent of their stabilities in solution.

Detecting the Dissociation of Compact Subunits

We used the optimized CDP conditions described above to screen the CID and CIU responses for a range of protein complexes in order to determine the charge states at which the CID threshold precedes the threshold for CIU. By definition, ions that undergo CID from states

that do not unfold must eject product ions that are similarly compact. During the course of our experiments, we assessed the relative stability of ions produced by charge reduction in solution using TEAA against those produced by CDP. In general, we found them to be equivalent, as shown for the 12+ charge state of the avidin tetramer (see *Supplemental Figure S8*).

To rapidly screen the CID and CIU energy landscape for protein complexes as a function of charge state, IM drift time data was monitored to determine the minimum collision energy at which CIU is observed. For this work, we define the CIU energy threshold as that energy at which a 2.5% increase in drift time/CCS relative to the smallest recorded value is observed. Figure 3a shows CCS values extracted from IM drift time data for 7^+ β-Lac dimer ions over an acceleration voltage range of 20 to 200V. We observe protein complex compaction with no observable unfolding over the energy range attainable. From this same data, protein complex CID can be monitored, and is shown in Figure 3b. As accelerating voltage used to active the ions is increased, we observe the relative intensity of the 7^+ dimer ion decrease while signals corresponding to the 3^+ and 4^+ monomer ions increase. At an accelerating voltage of 200 V, where we observe no precursor ion CIU, monomers account for more than 50% of the total ion intensity, indicating the CID threshold energy has been surpassed. Similar data was acquired for a range of protein complexes, including: β-Gal tetramer, β-Lac dimer, ConA tetramer, Hgb dimer and tetramer, SAP pentamer, and TPI dimer.

These data were combined with the threshold energies previously determined for avidin and aldolase tetramers[34] and for tetrameric transthyretin (TTR).[29] The identified charge states required for compact monomer ejection were then plotted as the *log*(protein charge state) against the intact mass of the precursor ion, plotted as *log*(protein mass), from the expected oligomer mass taken from the protein data bank (PDB), and the resultant plot is shown in Figure 3c. This

plot is highly linear, with an R^2 of 0.9892. From these data, the charge state required for compact protein monomer ejection from its precursor assembly in the gas phase can be predicted using the following equation:

$$CS = 0.012M^{0.62} \quad (1)$$

where M is the expected sequence mass of the protein complex. In Figure 3d, we use this equation to predict the charge state required for onset of the compact monomer CID pathway, and compare these predicted charge states to those determined experimentally. A one-to-one relationship is observed, exhibiting good agreement to a linear fit (R^2 = 0.9922), further supporting the predictive strength of Equation 1.

In order to evaluate the structure-relevant information content of the CID products generated via the compact monomer ejection pathway, we recorded CCS data for monomer product ions generated from the protein complex precursor charge states reported in Figure 3c and d. The analysis of this data is shown in Figure 4 for the following precursor ions: 7^+ β-Lac dimer (a), 10^+ TPI (b), 7^+ Hgb dimer (c – Hgb A and d – Hgb B, open circles), 11^+ Hgb tetramer (c and d, closed circles), 11^+ avidin (e), 15^+ ConA (f), 17^+ SAP (g), and 19^+ aldolase (h). Dashed lines on each plot indicated the theoretical CCS value predicted from the monomer extracted from the X-ray structure, as described previously.[35] While no clear trends that correlate ejected subunit CCS to X-ray predictions with respect to mass or parent ion CCS can be extracted from the data in Figure 4, we note that an average charge of 7.8 +/- 1.2 (1σ) is predicted to provide an experimental CCS having a near-zero residual to X-ray predictions for all systems studied here, assuming a near-linear relationship between ejected monomer CCS and charge state. This is a surprising observation, and one that indicates a general lack of defined structure in the product ions produced under any CID condition. In addition, we also detect general trends associated

with the symmetry of the charge partitioning associated with the product ions analyzed in Figure 4. In cases where more symmetric charge partitioning is observed, measured CCS values are smaller than those predicted (see Fig. 4a, c, d, e, and h), however in cases where charge partitioning is highly asymmetric, the measured CCS values are greater than those predicted (see Fig. 4b, c, d, f, and g), with the lowest charge state ions usually producing CCS measurements in closest agreement with X-ray based predictions. It is worth noting that, in cases where asymmetric charge partitioning-type CID was observed, the highest product ion charge state can exceed the parent ion charge, supporting a charge reduction mechanism that includes direct anion attachment to the precursor ion, thus facilitating facile charge stripping following collissional activation.[36]

Alternative Dissociation Pathways

For two systems studied in this report, we observed dissociation pathways that do not generally conform to the mechanistic expectations discussed above. For example, data for β-Gal is highlighted in Figure 3c (an open circle), as CID of compact precursor ions did not produce intact monomer product ions. CID of low charge state precursor ions generate product ions that are exclusively related to covalent bond fragmentation and peptide product ions.[29] As shown in Figure 5a, CID of the 35^+ charge state produces product ions with a measured mass of 34,800 ± 80 Da that we tentatively identify as an ion produced from monomer backbone dissociation. Based on data shown in Figure 5, we believe that this product ion contains around 300 residues out of the 1,021 total residues contained per intact monomer, but our mass accuracy and resolving power are current insufficient to confidently identify which region of the monomer is observed. Similar product ions are observed for higher charge states of β-Gal, for example the 47^+ shown in Figure 5b, where we observe a bimodal product ion distribution consisting of

32,870 ± 30 Da (similar to low charge state dissociation) and 47,450 ± 30 Da species. As for the CID product ions observed from charge reduced species, these likely correspond to large fragments of the intact β-Gal monomer (117 kDa), containing ~300 and 400 residues respectively. While dissociation of β-Gal does not apparently follow any CID pathway previously reported for protein complexes, we note that the product ions produced from charge reduced precursors carry less charge (~16%) than those generated from control spectra.

Similarly to β-Gal, we do not observe catalase tetramer precursor ions of any charge state to release compact monomers. Instead, low charge state precursor ions produce both unfolded monomer ions and heme-related product ions, as shown in the data for the 24^+ tetramer (Figure 6a). Similarly-produced heme ions generated during CID of Hgb allowed us to confidently identify the 616.2 m/z species as the apo heme co-factor. We identify an additional peak, 648.2 m/z, as the O_2 bound heme form, along with a number of other heme-associated signals. In contrast to charge reduced species, CID of the 33^+ tetramer (Figure 6b), produces low-intensity monomer peaks as well as four heme-related signals. Additionally, high-intensity signals are observed corresponding to a mass 19.5 kDa, a value which is approximately one-third the intact catalase monomer mass. Low intensity stripped-oligomer signals are also observed with a measured mass of approximately 214 kDa, which we assign as the catalase trimer bound to approximately two-thirds of a fourth catalase monomer. Similar to previous reports,[29] this is direct evidence of a backbone cleavage occurring within a single catalase subunit while bound to the tetramer, rather than evidence of a secondary dissociation event occurring following monomer ejection. It is worth noting that catalase and β-Gal are the two largest protein complexes included in this study. As such, caution should be taken when attempting to

extrapolate the trends observed here toward large protein systems, especially when such systems contain co-factors and non-protein binding partners.

Conclusions

Here, we have evaluated a CDP device as an effective method for generating lower charge states across a broad range of intact protein complexes under equivalent conditions. Following a detailed evaluation of the operation of the CDP device, we then utilized its ability to quickly produce large numbers of charge reduced protein ion signals to study the consequences of such charge reduced states on the CID pathway of intact protein complex ions. The low charge states produced were screened to identify those charge states for which the dissociation and unfolding threshold energies converge to the same value or invert to produce product ions before the onset of unfolding. The identified charge states show that CID-CIU convergence can be predicted to a high degree of accuracy based on precursor mass alone over a mass range of approximately 429 kDa. The product ions produced under such charge reducing conditions were largely compact, but also included product ions in the forms of unfolded monomers, large peptide/domain-level fragment ions, and charged co-factor release. All of these product ions have been reported previously in the literature from protein complex precursor ions,[29,37] however, the preferential backbone cleavage CID pathway from both low and native charge state precursor ions of β-Gal and catalase has not, and may pose a minor limitation for charge reduction protocols that seek compact protein product ions exclusively from CID. The closest analog of this β-Gal CID pathway was reported in the context of concanavalin A, however producing less massive peptide product ions that represent a more minor fragmentation pathway.38 While these data are somewhat preliminary, it is clear that surface induced

dissociation (SID),[39] in combination with charge amplification-CID and protein complex disruption in solution,[40] may be pooled with CDP-CID data in the fututure to provide a more complete assessment of protein subcomplexes and subunit sizes for modeling.[35] We also observe enhanced charge stripping following the collisional activation of charge reduced protein complex ions produced using the CDP source, which clearly points to a direct anion attachment mechanism for CDP protein charge reduction.

The work presented here builds substantially on previous data for charge reduced protein complex ions and their CID product ions. The predictive relationship presented in Equation 1 represents a potentially useful framework for high-throughput structural biology protocols, where monomer size information is often difficult to recover from solution disruption experiments alone. In addition, our data surprisingly reveals that ejected monomers with charge states ranging from 7^+-9^+ should represent those most-correlated to X-ray predictions for monomers having masses ranging from 16-39 kDa, providing an excellent starting point for modeling protein monomer subunit sizes in that mass range. It is highly likely that such an observation will be mass dependant if a wider range of proteins are included in the analysis; however, the data presented here suggests that such a broad correlation between ejected subunit mass and the charge state most-correlated to X-ray data will likely be relatively weak. Future work will be focused on broadening the available dataset of charge reduced protein CID data to include a greater number of large protein complexes that contain non-protein binding components and post-translational modifications, in order to more completely evaluate the breadth of the correlations provided in this report.

Acknowledgements

Funding for this work was supplied by the National Science Foundation (BTR, CAREER Award, 1253384).

Figure Captions

Figure 1. Mass spectra for denatured cytochrome C under various charge reduction conditions. In order to find the optimal conditions, under various (a) probe voltages with probe pressure held at 70 psi, (b) probe pressures with voltage held at -7250 V, and (c) source backing pressures with the probe voltage and pressure held at -7250 V and 70 psi, respectively. At higher probe voltages and pressures, greater levels of charge reduction are observed with decreased signal intensity. A compromise between charge reduction effectiveness and signal loss is made using the optimized conditions of -7250 V and 70 psi. At lower source backing pressures with sampling cone voltage at 200 V, in-source activation aids in stripping neutral and charge adductions, producing spectra with higher intensity peaks at lower charge states at higher resolution. To reduce structural effects due to in-source activation, the source backing pressure is raised to approximately 7 mbar for all intact protein complex, while maintain a sampling cone voltage of 200V.

Figure 2. Mass spectra from (a) β-lactaglobulin, (b) triosephosphase isomerase, (c) serum amyloid P, and (d) β-galactosidase with (top) and without (bottom) corona discharge probe turned on. The corona discharge probe has little effect on the charge state of the most abundant peaks across all complexes. The lowest charge states shift dramatically due to charge reduction, and in the case of SAP, the lowest charge state decreases by ten charges. β-lac CDP spectra have been deconvoluted using post-mobility data processing.

Figure 3. Representative data for β-lactaglobulin used to determine the charge state where CID and CIU threshold energies converge, and plots of all identified charge states from CID-CIU convergence screen. For 7^+ β-lactaglobulin the (a) CCS data show compaction consistent with other studies and no unfolding over the full energy range of the instrument, while (b) mass

spectra for different collision energies show the onset of monomer dissociation approximately 175 V. At 200 V, the monomer ion intensity accounts for more than 50% of the total ion intensity, indicating that the collision energy has exceeded the CID threshold energy. (c) Plot of *log* Protein Charge State verse *log* Protein Mass showing the linearity of the data for over mass range of 429 kDa (β-Lac (37 kDa) to β-Gal (466 kDa). (d) Plot of predicted protein charge states generated from the equation found in (c) against the observed protein charge states. This plot also shows good linearity between theoretical charge states and measured charge states in a near one-to-one relationship. β-galactosidase data (open circle in c and d) is highlighted since at the CID threshold generated product ions associated with monomer backbone cleavage of up to 300 residues.

Figure 4. Ejected monomer collision cross-sections for (a) β-lactaglobulin, (b) triosephosphate isomerase, (c) hemoglobin A, (d) hemoglobin B, (e) avidin, (f) concanavalin A, (g) serum amyloid P, and (h) aldolase. For hemoglobin, monomers were generated from dimers (open circles) and tetramers (closed circles). Dashed lines correspond to predicted CCS values from known oligomer crystal structures. In cases where measured CCS values are less than or within error to predicted values (a, c, d, e, h), dissociation proceeds via a symmetric charge partitioning pathways. While in cases where measured CCS values are greater than predicted values (b, c, d, f, g), dissociation proceeds via an asymmetric charge partitioning pathways

Figure 5. Mass spectra produced from dissociation of (a) 35^+ and (b) 47^+ β-galactosidase. Insets show blown up regions of product species produced from dissociation. For 35^+ β-Gal, dissociation produces a single species with a 17^+ to 19^+ charge distribution which has a measured

mass of 34,800 ± 60 Da, identified as a monomer backbone cleavage of containing around 300 residues. Similarly, CID data for 47^+ β-Gal produces two product ion populations having charge states between 19^+ and 24^+ as well as 21^+ and 27^+ with masses of 32,870 ± 30 Da and 47,450 ± 30 Da respectively, which are identified as product ions associated with β-Gal monomer backbone cleavage containing 300 and 400 residues, respectively.

Figure 6. Mass spectra produced from dissociation of (a) 24^+ and (b) 33^+ catalase. Insets show zoomed regions of product species produced from dissociation. For 24^+ catalase, CID produces two types of species. Monomers are produced with a charge state distribution ranging from 11^+ to 14^+. A second set of peaks in the low mass-to-charge region is observed with m/z values of 616.2 m/z, 619.2 m/z, 635.2 m/z, and 648.2 m/z are related to charged release of heme co-factors bound to catalase subunits. For 33^+ catalase, in addition to the same heme-associated peaks and low-intensity monomer peaks (with a charge state distribution ranging from 13^+ to 16^+), there are two additional distributions with charge distributions ranging from 13^+ to 15^+ and 17^+ to 21^+, which have measured masses of approximately 19.5 kDa and 214 kDa, respectively. The former distribution is identified as product ions associated with backbone cleavage of approximately one-third of the monomer while the latter distribution is identified as the complementary product ions, trimer bound to two-thirds of a fourth monomer.

Figure 1.

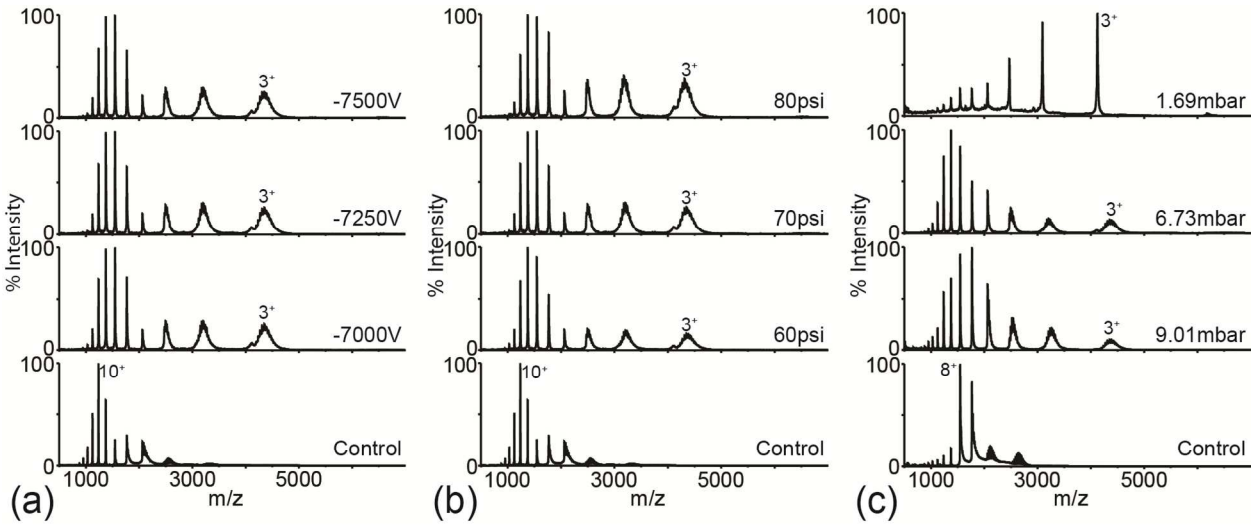

Figure 2.

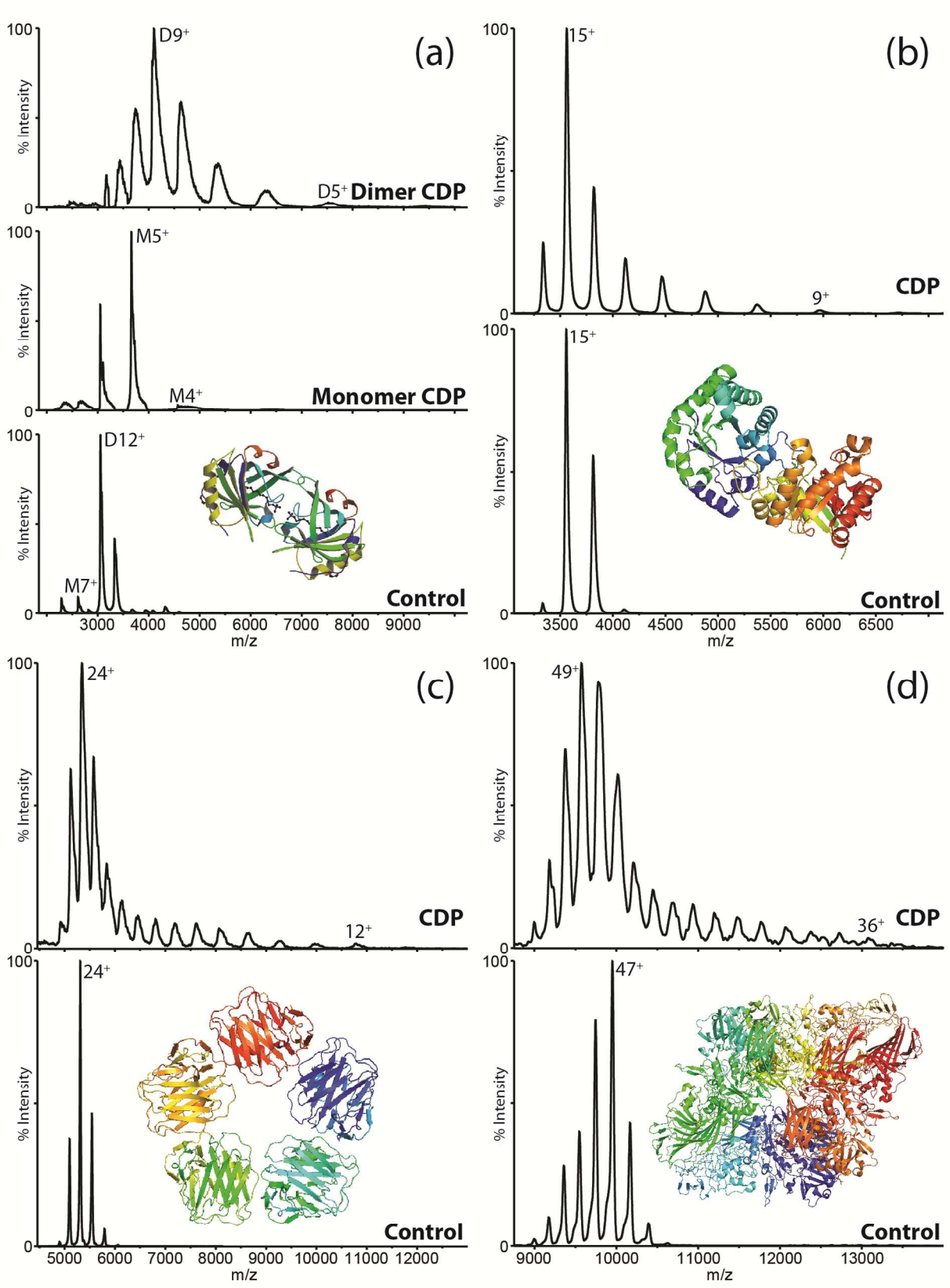

Figure 3.

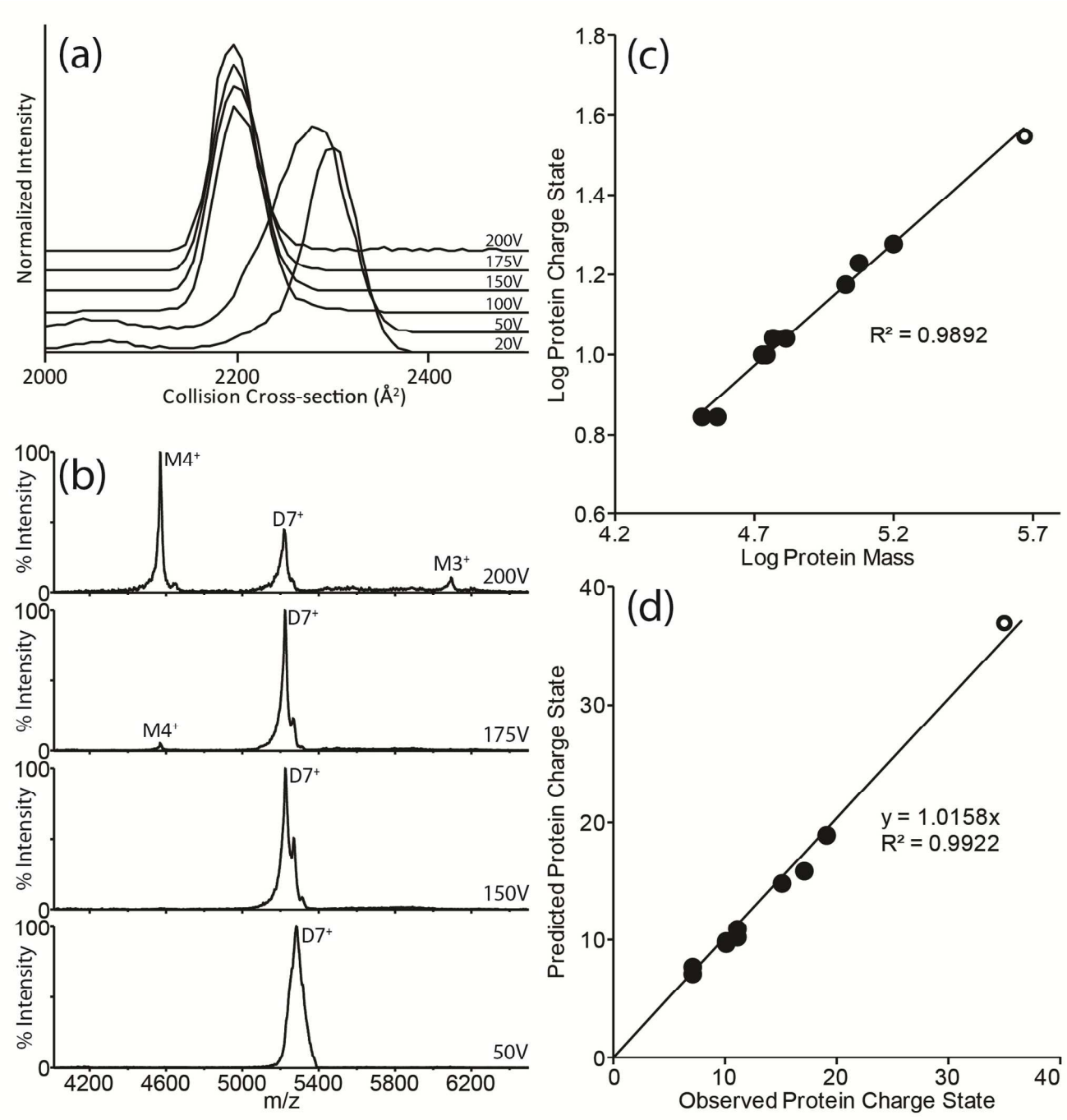

Figure 4.

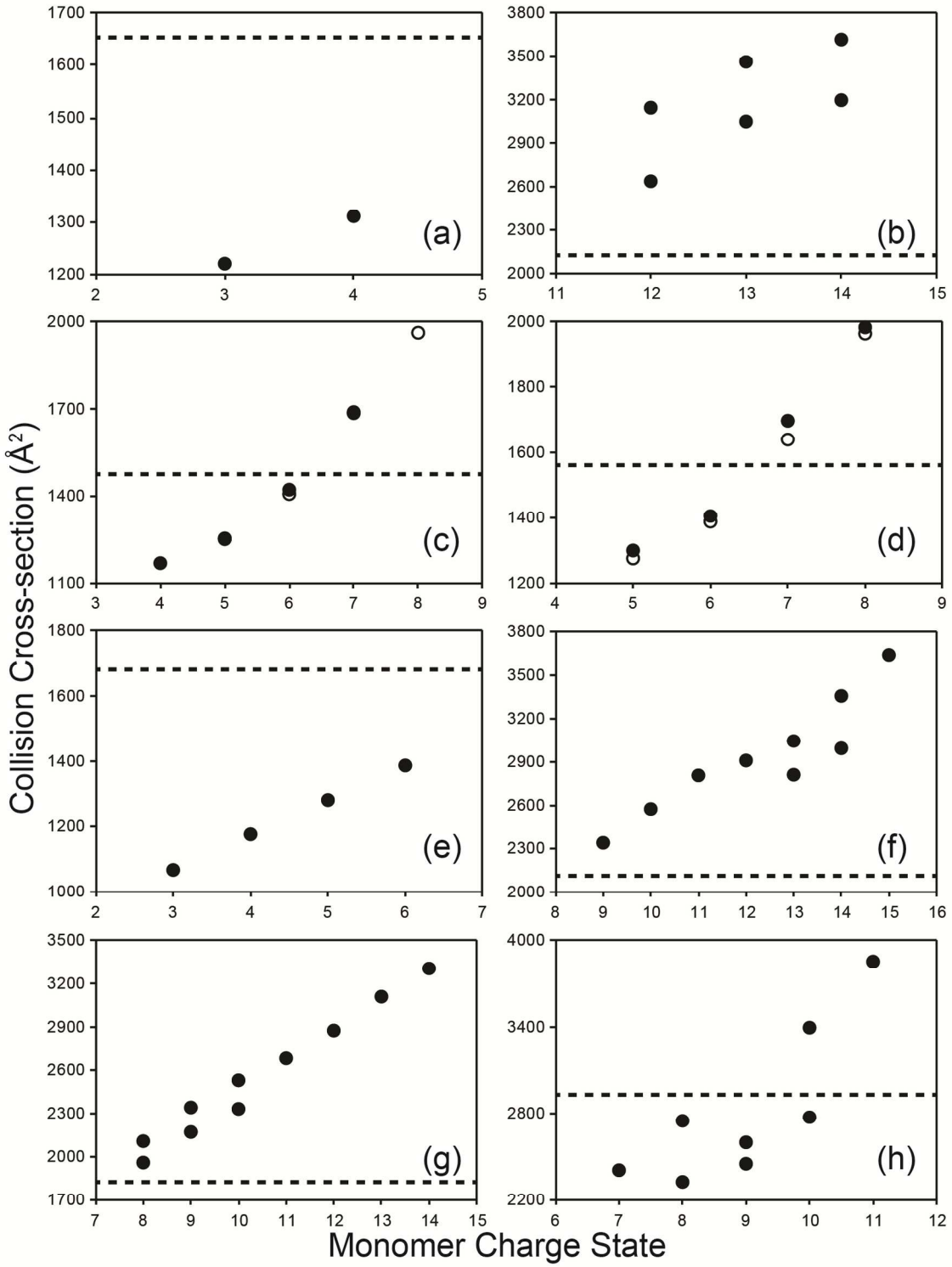

Figure 5.

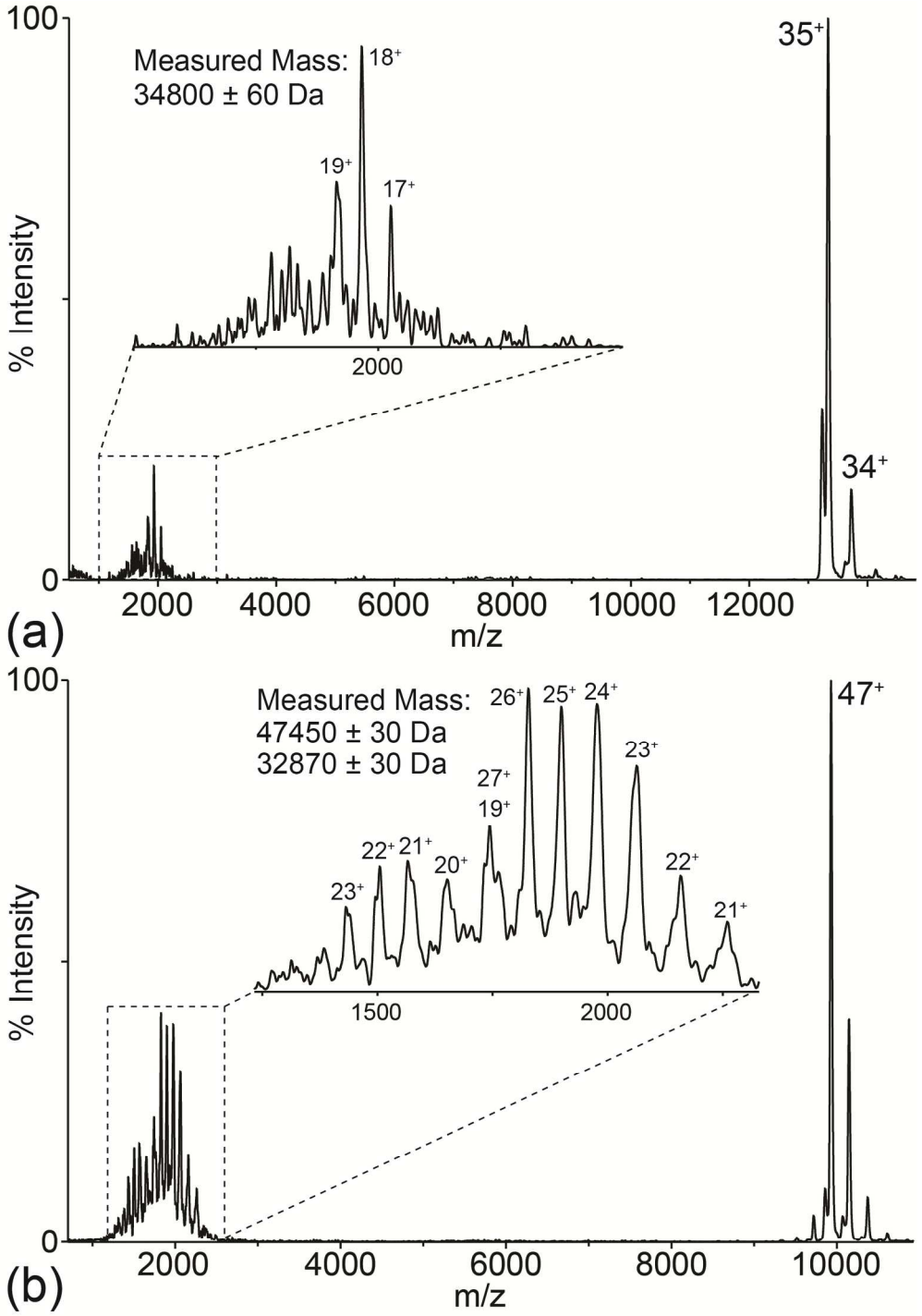

Figure 6.

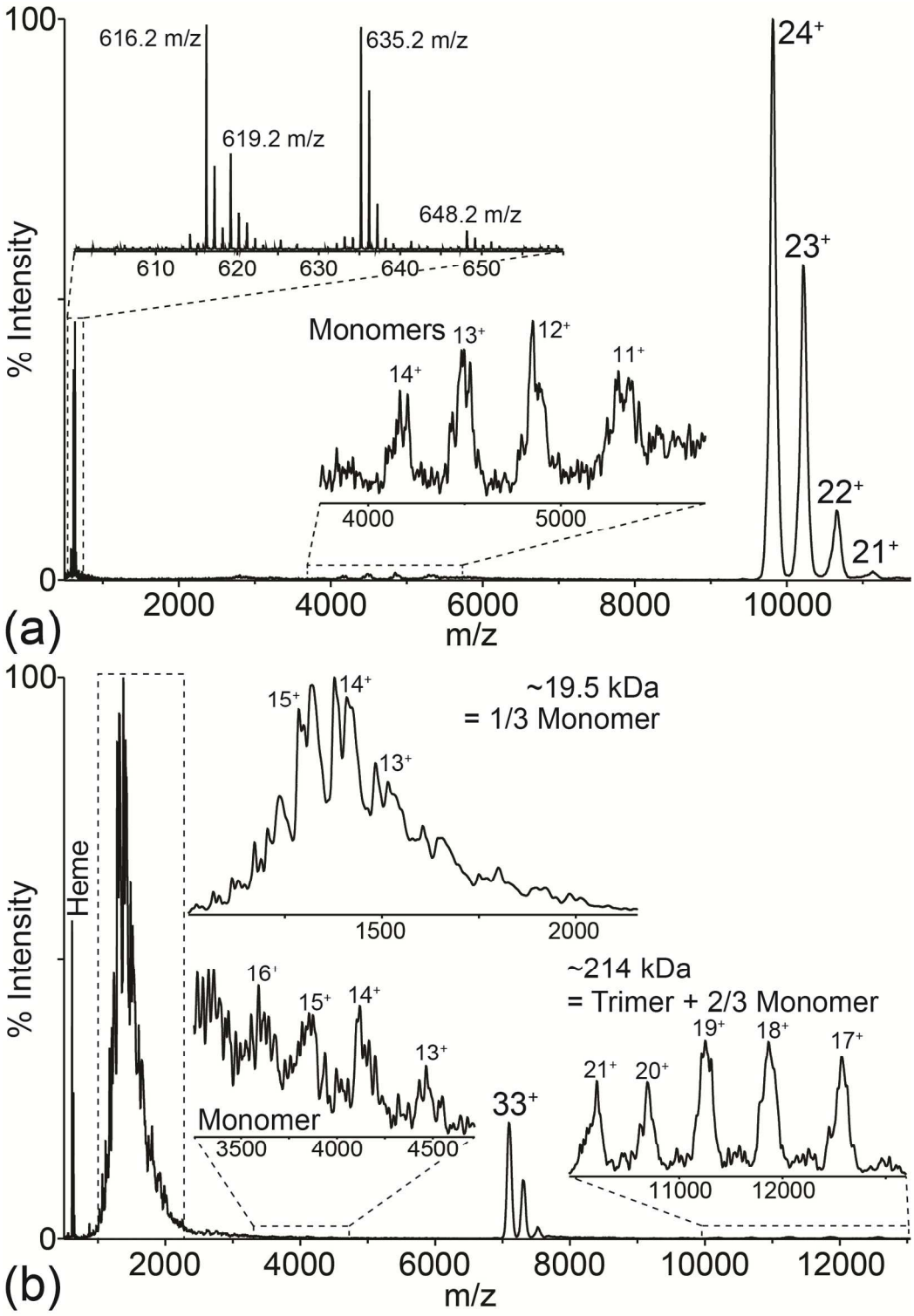

References

(1) Spirin, V.; Mirny, L. A. *Proc. Natl. Acad. Sci. U. S. A.* **2003**, *100*, 12123.

(2) Csermely, P.; Korcsmáros, T.; Kiss, H. J. M.; London, G.; Nussinov, R. *Pharmacology & Therapeutics* **2013**, *138*, 333.

(3) Jorgensen, W. L. *Science* **2004**, *303*, 1813.

(4) Loo, J. A. *Mass Spectrom. Rev.* **1997**, *16*, 1.

(5) Hyung, S.-J.; Ruotolo, B. T. *Proteomics* **2012**, *12*, 1547.

(6) Ruotolo, B. T.; Giles, K.; Campuzano, I.; Sandercock, A. M.; Bateman, R. H.; Robinson, C. V. *Science* **2005**, *310*, 1658.

(7) Kanu, A. B.; Dwivedi, P.; Tam, M.; Matz, L.; Hill, H. H. *J. Mass Spectrom.* **2008**, *43*, 1.

(8) Jin Lee, Y. *Molecular BioSystems* **2008**, *4*, 816.

(9) Leitner, A.; Walzthoeni, T.; Kahraman, A.; Herzog, F.; Rinner, O.; Beck, M.; Aebersold, R. *Mol. Cell. Proteomics* **2010**, *9*, 1634.

(10) Englander, S. W. *J. Am. Soc. Mass Spectrom.* **2006**, *17*, 1481.

(11) Engen, J. R. *Anal. Chem.* **2009**, *81*, 7870.

(12) Kaltashov, I. A.; Bobst, C. E.; Abzalimov, R. R. *Anal. Chem.* **2009**, *81*, 7892.

(13) Wilm, M.; Mann, M. *Anal. Chem.* **1996**, *68*, 1.

(14) Ruotolo, B. T.; Robinson, C. V. *Curr. Opin. Chem. Biol.* **2006**, *10*, 402.

(15) Leary, J.; Schenauer, M.; Stefanescu, R.; Andaya, A.; Ruotolo, B.; Robinson, C.; Thalassinos, K.; Scrivens, J.; Sokabe, M.; Hershey, J. *J. Am. Soc. Mass Spectrom.* **2009**, *20*, 1699.

(16) Hall, Z.; Politis, A.; Robinson, Carol V. *Structure* **2012**, *20*, 1596.

(17) Politis, A.; Park, A. Y.; Hyung, S. J.; Barsky, D.; Ruotolo, B. T.; Robinson, C. V. *PLoS One* **2010**, *5*.

(18) Pukala, T. L.; Ruotolo, B. T.; Zhou, M.; Politis, A.; Stefanescu, R.; Leary, J. A.; Robinson, C. V. *Structure* **2009**, *17*, 1235.

(19) Zhong, Y.; Feng, J.; Ruotolo, B. T. *Anal. Chem.* **2013**, *85*, 11360.

(20) Zhong, Y.; Hyung, S.-J.; Ruotolo, B. T. *Expert Rev. Proteomics* **2012**, *9*, 47.

(21) Hernández, H.; Dziembowski, A.; Taverner, T.; Séraphin, B.; Robinson, C. V. *EMBO reports* **2006**, *7*, 605.

(22) Levy, E. D.; Erba, E. B.; Robinson, C. V.; Teichmann, S. A. *Nature* **2008**, *453*, 1262.

(23) Zhou, M.; Sandercock, A. M.; Fraser, C. S.; Ridlova, G.; Stephens, E.; Schenauer, M. R.; Yokoi-Fong, T.; Barsky, D.; Leary, J. A.; Hershey, J. W.; Doudna, J. A.; Robinson, C. V. *Proc. Natl. Acad. Sci. U. S. A.* **2008**, *105*, 18139.

(24) Aquilina, J. A. *Proteins: Structure, Function, and Bioinformatics* **2009**, *75*, 478.

(25) Zhou, M.; Dagan, S.; Wysocki, V. H. *Angew. Chem. Int. Ed.* **2012**, *51*, 4336.

(26) Jurchen, J. C.; Garcia, D. E.; Williams, E. R. *J. Am. Soc. Mass Spectrom.* **2004**, *15*, 1408.

(27) Jurchen, J. C.; Williams, E. R. *J. Am. Chem. Soc.* **2003**, *125*, 2817.

(28) Ruotolo, B. T.; Hyung, S.-J.; Robinson, P. M.; Giles, K.; Bateman, R. H.; Robinson, C. V. *Angew. Chem. Int. Ed.* **2007**, *46*, 8001.

(29) Pagel, K.; Hyung, S. J.; Ruotolo, B. T.; Robinson, C. V. *Anal. Chem.* **2010**, *82*, 5363.

(30) Bornschein, R. E.; Hyung, S.-J.; Ruotolo, B. T. *J. Am. Soc. Mass Spectrom.* **2011**, *22*, 1690.

(31) Campuzano, I. G.; Schnier, P. *Int. J. Ion Mobil. Spec.* **2013**, *16*, 51.

(32) Ruotolo, B. T.; Benesch, J. L. P.; Sandercock, A. M.; Hyung, S. J.; Robinson, C. V. *Nat. Protoc.* **2008**, *3*, 1139.

(33) Bush, M. F.; Hall, Z.; Giles, K.; Hoyes, J.; Robinson, C. V.; Ruotolo, B. T. *Anal. Chem.* **2010**, *82*, 9557.

(34) Bornschein R. E.; Niu, S.; Eschweiler, J. E.; Ruotolo, B. T. **2015**, *In Press,* DOI: 10.1007/s13361-015-1250-7.

(35) Benesch, J. L. P.; Ruotolo, B. T. *Current Opin. Struct. Biol.* **2011**, *21*, 641.

(36) McLuckey, S. A.; Stephenson, J. L. *Mass Spectrom. Rev.* **1998**, *17*, 369.

(37) Versluis, C.; Heck, A. J. R. *Int. J. Mass Spectrom.* **2001**, *210–211*, 637.

(38) Han, L.; Ruotolo, B. T. *Int. J. Ion Mob. Spectrom.* **2013**, *16*, 41-50.

(39) Zhou, M.W.; Jones, C.M.; Wysocki, V.H. *Anal. Chem.* **2013**, 85, 8262.

(40) Hall, Z.; Hernandez, H.; Marsh, J.A.; Teichmann, S.A.; Robinson, C.V. *Structure* **2013**, 1325.